

Investigations on stability and performance of a variable frequency based fuzzy logic controller for induction cooking system

Pradeep Vishnuram ^{1*}, Booma Nagarajan ², A. Sureshkumar ¹

¹ Assistant Professor, SRM University, Chennai, Tamilnadu, India

² Professor, Jerusalem College of Engineering, Chennai, Tamilnadu, India

*Corresponding author E-mail: Pradeep.kannan03@gmail.com

Abstract

Load variability and perturbation is an important issue in the induction cooking applications as it hinders the performance of the heating system considerably. Therefore a precise power control technique is required for induction heating applications by considering the stability issues and dynamic response of the system. Also, the safety operating ranges need to be confirmed to ascertain the competency of the controller. In this paper, a Fuzzy logic based power control scheme is introduced by considering the load uncertainties. The suggested power control technique uses variable frequency control of the inverter for reaching the target power level. Also, a detailed stability study is done for investigating stability range within which the system operation is safe and stable. The said work is simulated in MATLAB/Simulink environment and realized as a prototype where advanced FPGA controller renders its hand. The simulation and hardware results reveal that the suggested technique is versatile.

Keywords: Induction Cooking; Stability; Modelling; Fuzzy Logic Controller; Dynamics; Power Control.

1. Introduction

In induction cooking (IC) applications, the effective heat transfer from source to pot happens only when there is adept power regulation mechanism. The most commonly used electronic converter for domestic induction appliances is the series resonant class D inverter, shown in Fig.1, where an inductor-vessel set is considered to be the load, which is represented with its equivalent R_{eq} - L_{eq} . The values of the R_{eq} - L_{eq} gets varied due to change in the temperature, the switching frequency f_{sw} and the vessel material's electromagnetic properties [1]. N. Ha Pham et.al, suggested a power control scheme where the output of series resonant inverter (SRI) is controlled by the dc link voltage. This technique uses two loops: one to track the resonant frequency of the load by adjusting the inverter f_{sw} and other by controlling the magnitude of the dc link voltage [2]. The employment of dual control loop resulted in high cost and increased complexity.

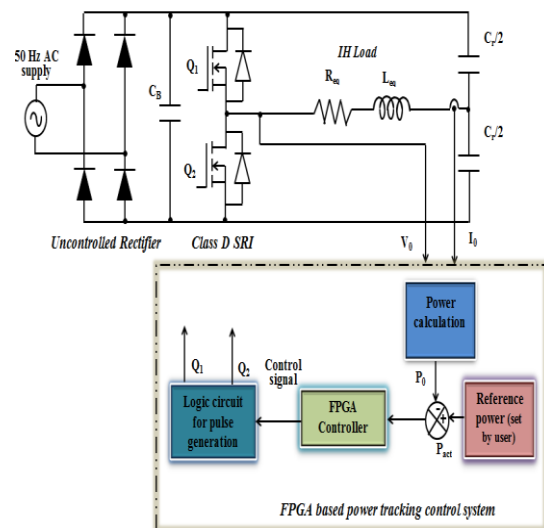


Fig. 1: Schematic of the Class D Resonant Inverter Based IC System.

When an uncontrolled diode bridge rectifier is used for feeding the inverter, the control over the dc link voltage is not possible and also requires higher value of dc-link capacitor to make input voltage to be ripple free dc. In such cases, different phase control methods are used to have a control between the output voltage and current. In [3], [4], the dual control loop is employed for full bridge inverter with Phase-Shift modulation technique. Here the first loop adjusts the f_{sw} which guarantees the Zero Voltage Switching (ZVS) and the second loop adjusts the firing angle of the rectifier in accordance with the output power regulation. The

same control technique is used in [5], for half bridge inverter to regulate the output power with ZVS. Pulse Density Modulation (PDM) based power control is proposed in [6], [7] with constant f_{sw} . C. Branaset al, enhanced the control technique considering other issues like flicker and temperature ripples. Even though this method is easy for power control, some standards like flicker emissions [8] and temperature ripple needs to be considered.

In order to improve the power factor, the rippled dc link voltage is applied to the inverter which also reduces the cost of the system relatively. In such cases, phase control is not feasible at inverter side as it is tricky to determine zero crossing from the measured current. To alleviate this issue, a control logic is designed with real and imaginary current, voltage component [9] whereas O. Lucia et.al., employed a discontinuous mode control [10]. Research papers on maximum power tracking mechanism like perturb and observe (P&O) in renewable power sources, where the peak power is extracted through fixed step variation influenced researchers to try similar mechanism in IC applications [11-14]. In order to maintain ZVS and to avoid peak overshoots, the fixed step size needs to be smaller. But in turn it increases the settling time and results in poor responses under load uncertainties. Thus a variable step size could be used to avoid such problem [15]. In [16], gain scheduled PI controller is proposed with the dynamic model of the system.

This paper put forth a FLC based power control scheme for IC and the objective of this work is to develop a closed loop power control scheme using FLC to deliver the set power for wide range of IC loads. And also to determine the safe operating range by considering the load uncertainties.

The paper is well structured as follows: section 2 consists of mathematical modeling of resonant inverter with state space analysis. Section 3 deals with stability analysis of the SRI using nyquist plot to identify the safe operating range. FLC based power control is clearly dealt in section 4. Section 5 discusses the results fetched through simulation, Section 6 presents the main experimental results used to validate the converter operation and conclusion is provided in section 7.

2. Mathematical model of resonant inverter

2.1. State space model of the class – d inverter

The output power transferred to the load is deduced using Fourier series and is given by

$$P = \frac{R_{eq}}{2} \frac{(2V_m \sin(\pi D) / \pi)^2}{R_{eq}^2 + (L_{eq} \omega_{sw} - 1 / (C_r \omega_{sw}))^2} \quad (1)$$

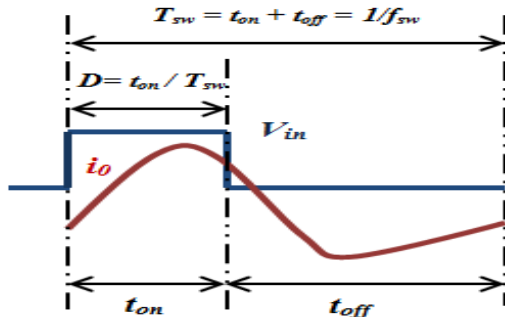


Fig. 2: Switch Voltage and Load Current.

Where $\omega_{sw} = 2\pi f_{sw}$ is the angular switching frequency. The normalized frequency is given by $f_n = f_{sw}/f_0$.

$$\omega_0 = \frac{1}{\sqrt{L_{eq} * C_r}}$$

is the angular resonant frequency. Fig. 3 illustrates the normalized power graph as the function of the f_{sw} for various duty cycles D.

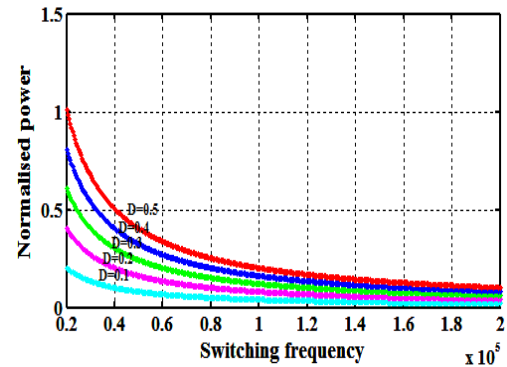


Fig. 3: Normalized Power Graph as the Function of the F_{sw} with Respect to the Various Operating Points.

The developed small signal modelling of the inverter could be expressed as state space equation as listed in [17]

$$\dot{x} = Ax + B \quad (2)$$

$$y = Cx \quad (3)$$

Where

x is the input state vector.

y is the output state vector.

$$x = \begin{bmatrix} \hat{i}_c \\ \hat{i}_s \\ \hat{v}_c \\ \hat{v}_s \end{bmatrix}^T \quad (4)$$

Where \hat{i}_c , \hat{i}_s , \hat{v}_c , \hat{v}_s are the perturbed real and imaginary voltage $v(t)$ and current $i(t)$ respectively.

The state variable matrix of the system is given by

$$A = \begin{bmatrix} \frac{-R_{eq}}{L_{eq}} & \omega_s & \frac{-1}{L_{eq}} & 0 \\ -\omega_s & \frac{-R_{eq}}{L_{eq}} & 0 & \frac{-1}{L_{eq}} \\ \frac{1}{C_r} & 0 & 0 & \omega_s \\ 0 & \frac{1}{C_r} & -\omega_s & 0 \end{bmatrix} \quad (5)$$

$$B_d = \frac{\sqrt{2}V_m}{L_{eq}} [\cos(2\pi D) \quad \sin(2\pi D) \quad 0 \quad 0]^T \quad (6)$$

$$B_\omega = [-i_s \quad i_c \quad -v_s \quad v_c]^T \quad (7)$$

The gain of the small signal duty-to-output power $G_{pd}(s)$, and frequency-to-output power, $G_{pf}(s)$, are obtained by the linearized state space model and is given by

$$\hat{p}_{pd}(s) = \frac{\hat{p}}{\hat{d}} = C(sI - A)^{-1}B_d \quad (8)$$

$$\hat{p}_{pf}(s=0) = \frac{R_{eq}}{2} \frac{(\sqrt{2}V_m)^2 \sin(\pi D) / \pi}{R_{eq}^2 + (L_{eq} \omega_{sw} - 1 / (C_r \omega_{sw}))^2} \quad (9)$$

$$\hat{p}_{pf}(s) = \frac{\pi * \hat{p}}{\omega_{sw}} = 2\pi C (sI - A)^{-1} B_\omega \quad (10)$$

$$\frac{V_{in}}{V_{out}}(s=0) \tag{11}$$

$$= \frac{-R_{eq}}{2} \frac{(\sqrt{2}V_{in})^2 \sin(\pi D) / \pi}{R_{eq}^2} \frac{1}{((L_{eq} \omega_{sw})^2 - (1/(C_r \omega_{sw}))^2) + (L_{eq} \omega_{sw} - 1/(C_r \omega_{sw}))^2}$$

Where

$$C = [R_{eq} I_s \quad R_{eq} I_c \quad 0 \quad 0]^T$$

The quality factor (Q) the coil is

$$Q = \frac{\omega_0 * L_{eq}}{R_{eq}} \tag{12}$$

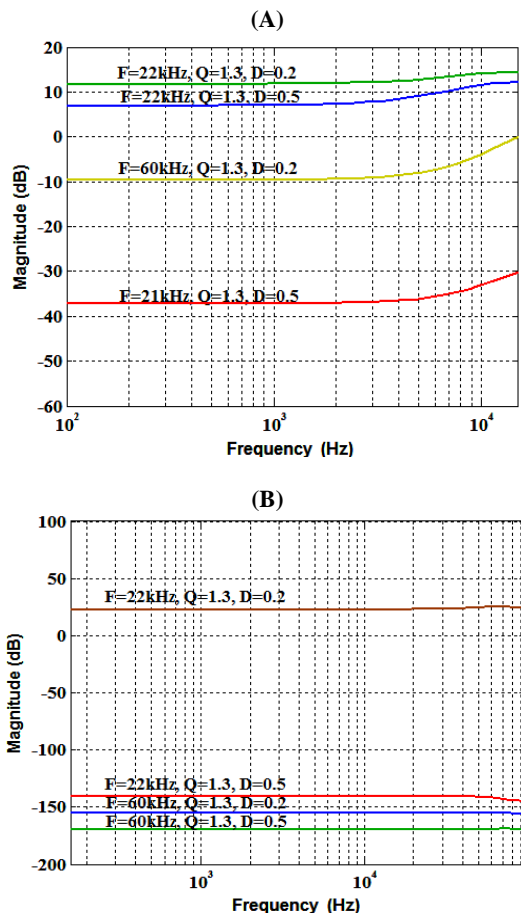


Fig. 4: (A) Magnitude Plot of G_{pd} with Various Operating Condition (B) Magnitude Plot of G_{pf} with Various Operating Condition.

Whenever the load parameters R_{eq} - L_{eq} changes, the parameters like duty cycle and frequency are need to be changed. Fig.4 shows the magnitude plots of G_{pd} and G_{pf} for the different operating conditions. The clear inference is that the dynamic behaviour and the closed loop stability of the inverter changes with respect to switching frequency and duty cycle. Therefore it is mandatory to locate the stability margins within which the operation is stable.

3. Stability analysis of the class-d inverter

With the help of the small signal model, the dynamic behaviour of the converter with respect to various operating conditions is studied and the open loop system is developed. The stability margin is obtained by using the nyquist plot for the developed mathematical model.

From the small signal modeling, the output power equation is presented as

$$P_0 = \frac{-R_{eq}}{2} \frac{\sqrt{2}V_{in}^2 \sin(\pi D) / \pi}{R_{eq}^2} \frac{1}{((L_{eq} \omega_{sw})^2 - (1/(C_r \omega_{sw}))^2) + (L_{eq} \omega_{sw} - 1/(C_r \omega_{sw}))^2} f_{sw} \tag{13}$$

From Eqn 13, it is very clear that the output power depends on the switching frequency. Thus the output power could be controlled by varying switching frequency. The control range of the frequency should be determined in order to ensure the system stability.

3.1. Nyquist stability criterion

The developed state space equation is converted into transfer function for analysing the closed loop system stability. The gain of the system is varied to check the stable operating points. The gain of the sensor (R(s)) is given by

$$R(s) = \frac{V_{in}}{V_{out} + V_{in}} \tag{14}$$

Here, a sample of the output power is fed as input to the controller. A simple, low cost potential divider arrangement is sufficient to sense and give feedback, the gain of the feedback element H(s) is given by

$$H(s) = \frac{V_{in}}{V_{out} + V_{in}} \tag{15}$$

The mathematical model of the closed loop controlled IH system for cooking applications is shown in Fig. 5. The gain of the PI controller C(s) is given by,

$$C(s) = K_p + \frac{K_i}{s} \tag{16}$$

The gain of the class D inverter T(s) with respect to constant supply voltage V_{in} for frequency control is given by [16]

$$T(s) = \frac{\sqrt{2}}{\pi} f_{sw} \tag{17}$$

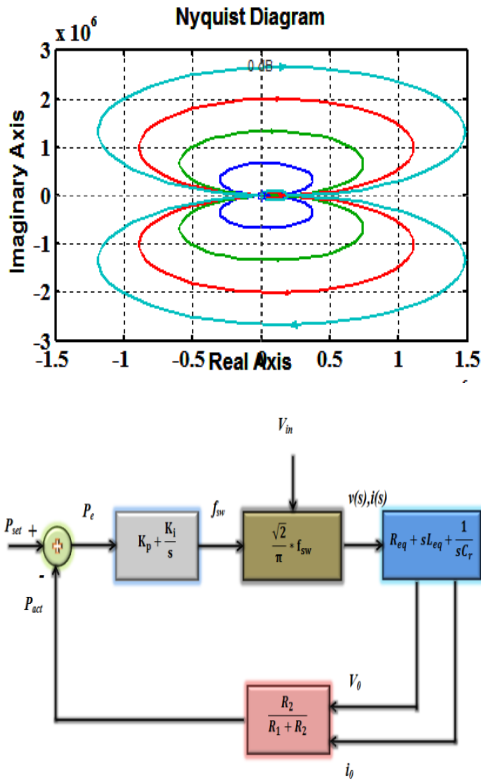


Fig. 5: Mathematical Representation of IH Supply with Conventional Controller.

The gain of the series resonant tank $O(s)$ is given by

$$O(s) = \frac{L_{eq}}{s} \{S^2 + Ms + N\} \quad (18)$$

Where

$$M = \frac{R_1 + R_2}{\omega} \quad (19)$$

$$N = \frac{1}{\omega^2 C_r} \quad (20)$$

From the Fig. 6, the transfer function of the system is given by

$$J(s) = \frac{G(s)}{1 + G(s)H(s)} \quad (21)$$

Where

$$G(s) = C(s)T(s)O(s) = \frac{C_r}{S^2} \{K_p S^3 + (K_p M + K_i) S^2 + (K_p N + K_i M) S + N K_i\} \quad (22)$$

$$H(s) = \frac{R_1 + R_2}{R_1 + R_2 + sL_{eq}} \quad (23)$$

By sub Eqn (22 and 23) in Eqn (21) and simplifying, the overall systems transfer function is given by

$$J(s) = \frac{K \{S^3 + X S^2 + Y S + Z\}}{S^3 + X (R_1 + R_2) \pi S^2 + Y S + Z} \quad (24)$$

Where

$$X = \frac{MK_p + K_i}{K_p} \quad (25)$$

$$K = f_{sw}$$

$$Y = \frac{NK_i}{K_p} \quad (26)$$

$$Z = \frac{NK_p + MK_i}{K_p} \quad (27)$$

Here K is the stability constant which is equal to the switching frequency of the inverter. The variation in the K determines the stable operating point of the inverter, which could be ensured by using the nyquist plot. For various values of the K , the nyquist plot is shown in Fig. (6).

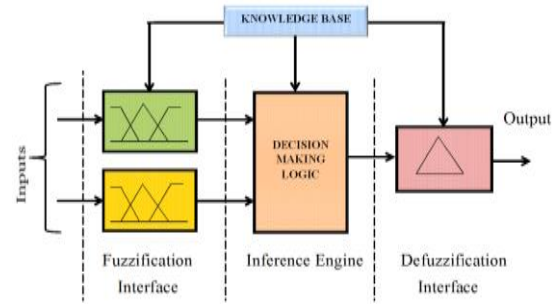


Fig. 6: Nyquist Plot for Various Values of K .

In order to track the stable operating point, the stability constant K is varied between 10 kHz to 226 kHz and it is observed that the closed loop remains stable. When the frequency is varied above 226 kHz, it is found that the closed system becomes unstable. Thus the controller should be able to generate the switching frequency between 10 kHz to 226 kHz, in order to track the set power and to ensure the system stability.

4. FLC based power control technique

FLC is a dynamic and intelligent tool to solve non-linear problems. As like conventional controller, FLC does not require the mathematical model of the system. For framing the rule base, it is necessary to understand the complete system with its control requirement. The FLC is designed using the information/data flow as input, it is then processed with decision making engine and its corresponding control signal is obtained with defuzzification engine. The three important stages are shown as block diagram in Fig. 7

With the v_o and i_o , the output power (P_o) is calculated and it is then compared with set power (P_{set}). The error in power (P_e) and its derivative (ΔP_e) are multiplexed and given as the input to the FLC. The control signal from the FLC is then given to the logic circuit for generating the high frequency pulses. The generated variable frequency pulses are given to the switches Q_1 and Q_2 in order to track the set power.

The inputs to FLC divided into seven membership functions as exposed in Fig. 8. They are labeled as NS (Negative Small), NM (Negative Medium), NL (Negative Large), VLN (Very Large Negative), Z (Zero), PS (Positive Small), PM (Positive Medium), PL (Positive Large), VLP (Very Large Positive).

Without considering the mathematical model of plant, fuzzy control rules have been developed through the basic control knowledge. The fuzzy rule base is given in the Table 1. The control action is performed with the help of the simple linguistic rules as tabulated in rule base. The corresponding surface plot is shown in Fig. 9. The flow chart for the controller action is shown in Fig.10.

5. Simulation results

The performances of the conventional PI controller and intelligent Fuzzy logic controllers are evaluated using MATLAB/Simulink for the load parameters as listed in Table 2. The PI controller and FLC are developed as per the above descriptions with its design specifications. For the load RL₁ the set power is 3700W. The simulation result of 3700W set power with conventional PI controller is shown in Fig. 11 (a). It is clear from the graph that the PI controller takes 0.05s to reach the target i.e, P_{set}. And it is also observed that, the response of the controller is an oscillating toward the set value with 8% steady state error. This is because of the non-linearity of the controller.

Fig. 7: Block Diagram of FLC.

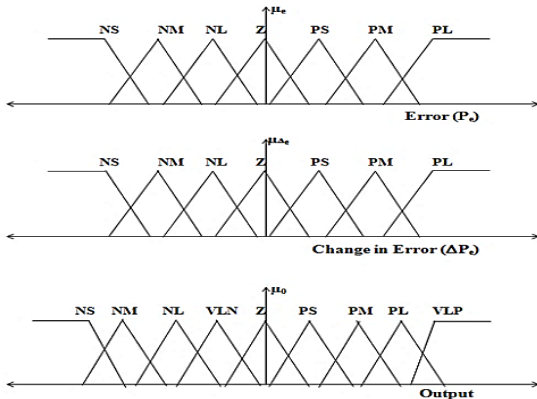


Fig. 8: Membership Functions of Input and Output Variables.

Table 1: Fuzzy Rule Base

P _e /ΔP _e	NS	NM	NL	Z	PS	PM	PL
NS	PL	PM	PM	NL	VLN	PS	NS
NM	PS	NM	VLN	PM	NL	Z	NL
NL	PS	PM	Z	NL	PL	NS	NS
Z	PL	NL	NM	PL	VLP	PS	Z
PS	PM	NM	NS	NL	Z	PS	NL
PM	VLN	NS	NM	PM	PS	Z	VLP
PL	VLP	PS	PL	VLN	PM	PL	VLN

Table 2: Load Parameters

Parameters	RL1	RL2	RL3
Resistance (Ω)	1.5	1.85	2.3
Inductance (μH)	26	10.5	16
Resonance frequency f _r (kHz)	22	35	28
Switching frequency f _{sw} (kHz)	23	36	29
Resonance capacitance (μF)	2		
RMS input voltage (V)	230		
DC link capacitor (μF)	2200		

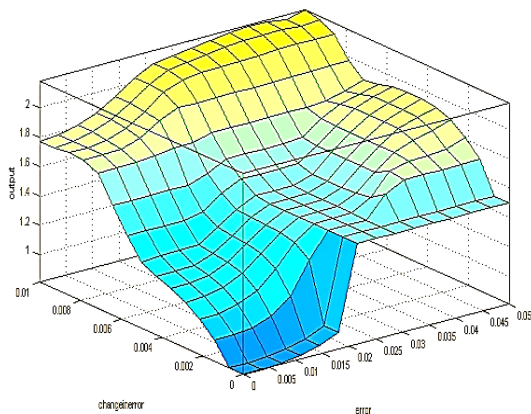


Fig. 9: Surface Plot of the FLC System.

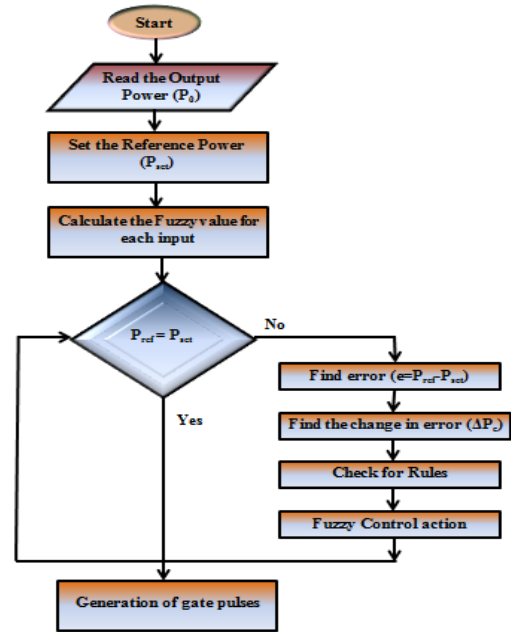


Fig. 10: Flow Chart of FLC Controlled System.

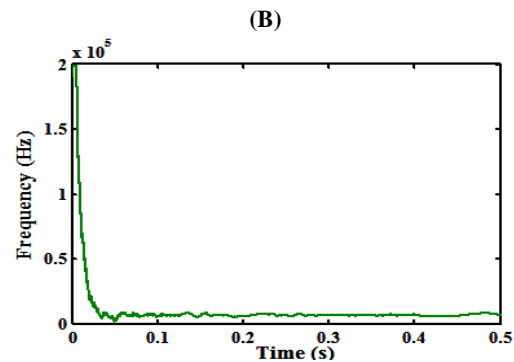
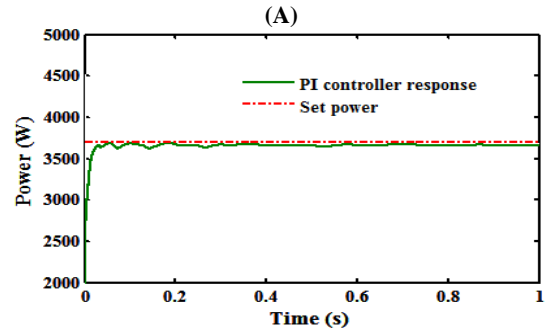


Fig. 11: Simulation Results for Load RL₁, P_{set}= 3700W (A) P_{set} and P_o with PI Controller (B) F_{sw} Time Evaluations.

In order to track the set power with the variation of the frequency with respect to time is shown in Fig. 11(b). In stability point of view, it observed that the closed loop system is stable within the frequency range of 10 kHz to 226 kHz. The stability operation of the closed loop could be ensured if the controller is operated within the frequency range as discussed in the section 2. The response of PI controller in accordance with the frequency control is found to be an oscillatory towards its set value. For the same control objective, the response of the PI controller and FLC are shown in Fig. 12(a). The conventional controller finds it hard to settle at the set point without oscillations and also it possess transient period. On the other hand FLC has a clear edge over its conventional counterpart in achieving the set value within an allowable transient period say 0.001s. Thus the net steady state error value is less than 0.1% for the same P_{set} with FLC. Fig. 12(b) illustrates variation of frequency for the set power with FLC. It is also observed

that, the response of the FLC on the frequency control is smoother than the conventional controller for the same load RL₁.

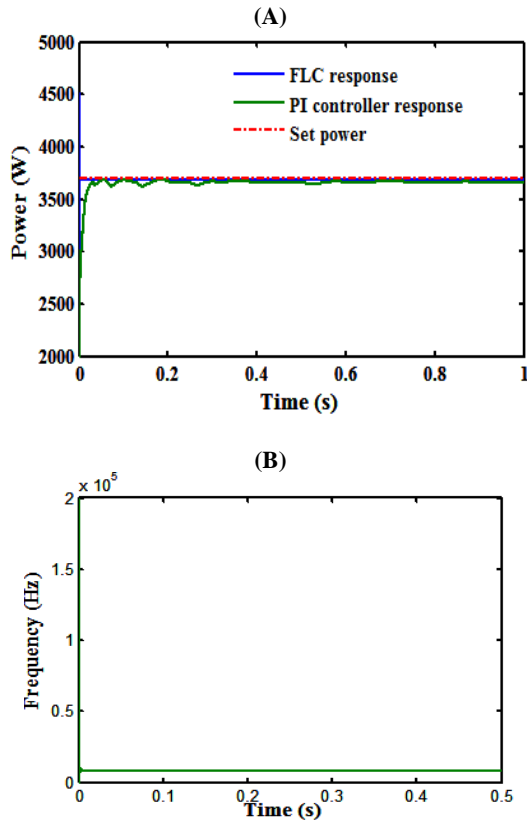


Fig. 12: Simulation Results for Load RL₁, P_{set}= 3700W (A) P_{set} and P_owith Various Controllers (B) F_{sw} Time Evaluations with FLC.

In order to validate the response of the controllers, the load and set power is varied. Change in load is RL₂ and P_{set} =1350W. It is observed that, the PI controller takes about 0.1s to reach the reach the target level with small peak overshoots. The output waveform is more oscillating toward the set power. Fig 13(a) shows the output power waveform for change in load. Comparing to Fig. 11(a), the response of the conventional controller is more oscillating with larger steady state error for change in load parameters. The variation of frequency with respect the PI controller response is shown in Fig. 13(b).

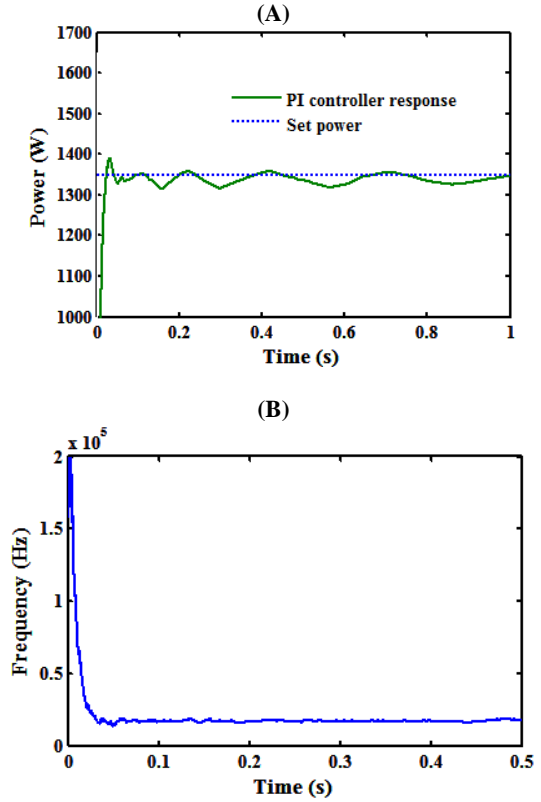


Fig. 13: Simulation Results for Load RL₂, P_{set}= 1350W (A) P_{set} and P_o with PI Controller (B) F_{sw} Time Evaluations.

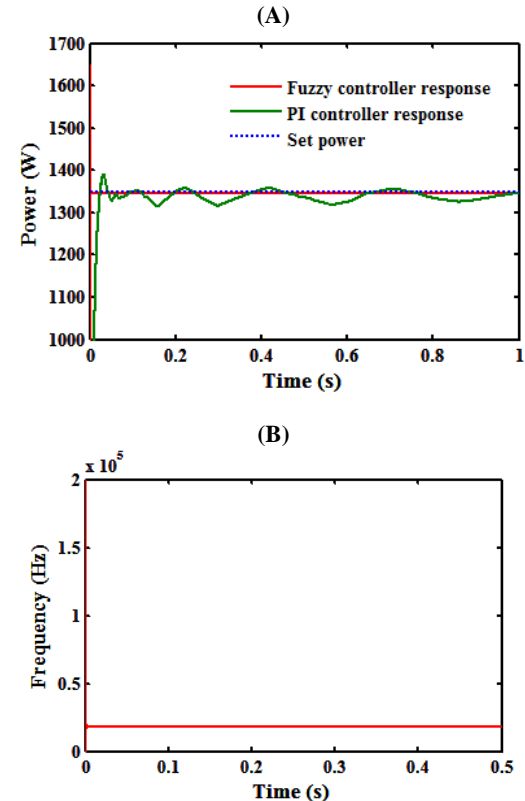


Fig. 14: Simulation Results for Load RL₂, P_{set}= 1350W (A) P_{set} and P_owith Various Controllers (B) F_{sw} Time Evaluations with FLC.

The suggested FLC is versatile for changes in load parameters and set power values. Here in this study the performance of FLC is tested for a change in load of RL₂ and set power P_{set}= 1350W. Fig 14(a) reveals that FLC is competent enough to achieve the set targets. The variation of the frequency with respect to time to track the set power is shown in Fig. 14(b). The comparison of both con-

trollers in power control of IC with respect to time domain specifications is shown in the Table 3.

Table 3: Comparisons of Time Domain Specifications

Load	Power (W)	Specifications	Controllers	
			PI	FLC
RL ₁	3700	Settling time (s)	0.05	0.00002
		Steady state error (W)	20	0.1
	1350	Settling time (s)	0.12	0.00001
		Steady state error (W)	24	0.15
RL ₂	900	Settling time (s)	*	0.0000135
		Steady state error (W)	*	0.2
	3700	Settling time (s)	**	0.00023
		Steady state error (W)	***	0.5
RL ₂	1350	Settling time (s)	0.23	0.00014
		Steady state error (W)	17	0.28
	900	Settling time (s)	**	0.05
		Steady state error (W)	***	0.42

*Too high for fixed gains ($K_p=0.368$ and $K_i=1.25$) for various set power.
 **Too high for fixed gains ($K_p=2.3$ and $K_i=0.58$) for various set power.
 ***Oscillating to its set level

6. Experimental results

In order to validate the simulation results, an experimental prototype addressing IC application has been developed. The control process is carried out through an advanced FPGA controller. The use of FPGA facilitates handy interaction with a simulation software environment say MATLAB/simulink which in turn minimise the time spent on hardware design. The switching pulses are generated with the dead time of 500ns and the power is measured using power analyser. The signal obtained by the power analyser is controlled by the PC via RS 232 cable. FLC has been defined in a MATLAB file. Circuit diagram of the proposed FPGA controlled IH system is shown in Fig 15.

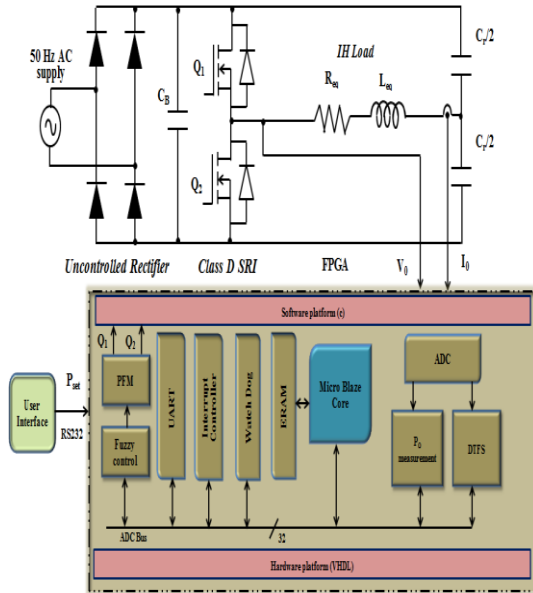


Fig 15: FPGA Implementation of the Proposed Fuzzy Logic Controller.

The FLC calculates the controlling parameter (f_{sw}) and it is transferred to FPGA via the serial communication port and thereby executes the control process. The experimental setup is tested with both PI controller and FLC and the time domain comparisons are listed in Table 3.

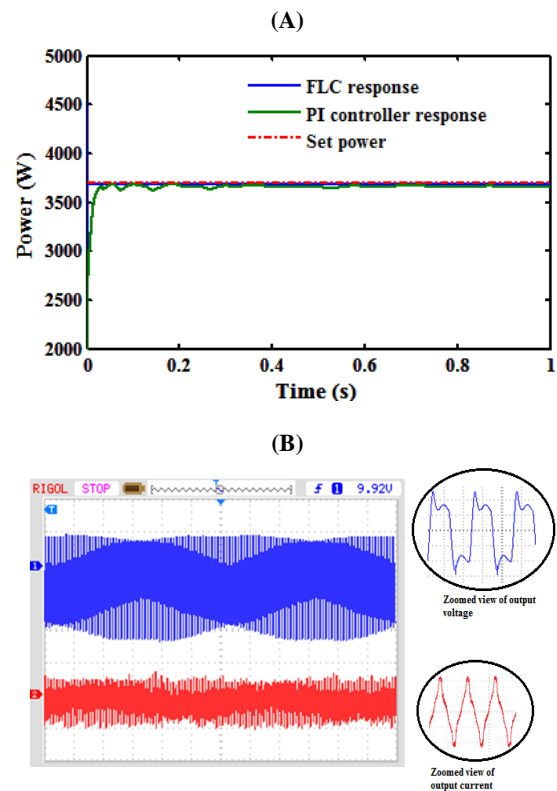


Fig 16: Hardware Results for $P_{set}=3700W$ for RL1: (A) Output Power Waveform Output Waveforms with PI and FLC Calculation (B) V_0 (Blue) 200 V/Div and I_0 (Red) 15 A/Div, 10 Ms/Div, at the Target Set-Point.

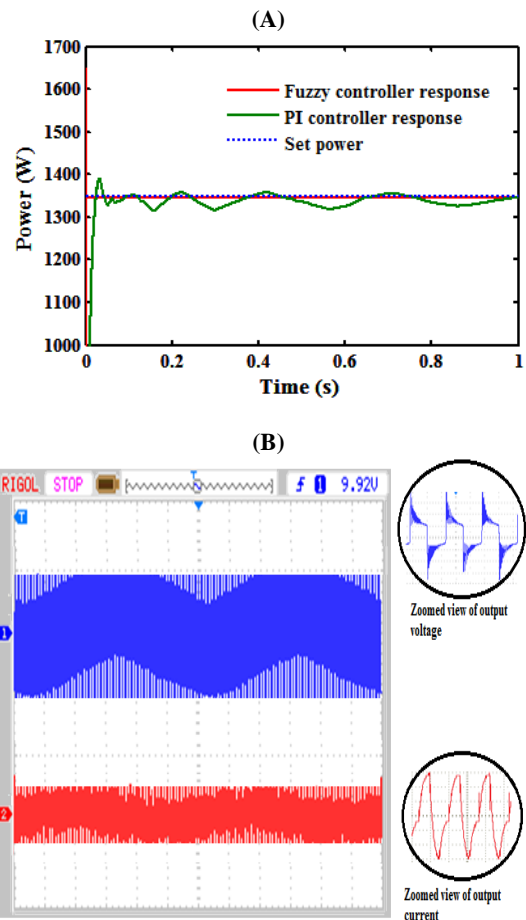


Fig 17: Hardware Results for $P_{set}=1350W$ for RL1: (A) Output Power Waveform Output Waveforms with PI and FLC Calculation (B) V_0 (Blue) 100 V/Div and I_0 (Red) 8 A/Div, 10 Ms/Div, at the Target Set-Point.

Fig 16(a) and Fig 17(a) signifies the response of PI controller and FLC for the set power of 3700W and 1350W respectively. Fig 17(b) shows the FLC controlled output voltage and current waveform with the set power of 3700W for the load $R=1.5\Omega$, $L=26\ \mu\text{H}$ and $C_f=2\ \mu\text{F}$, similarly Fig 17(b) shows the FLC controlled output voltage and current waveform with the set power of 1350W for the load $R=1.85\Omega$, $L=10.5\ \mu\text{H}$ and $C_f=2\ \mu\text{F}$. The zoomed waveform of the corresponding voltage and current is shown in the right pane. From the Table 3, it can be concluded that the error in steady state power and settling time is less in FLC controlled IC system. The experimental results shows that FLC controlled IC system has improved transient response and dynamic response.

7. Conclusion

Obtaining the safe operating range for the resonant converter with varying load is a challenging task and it is required to optimise the transient behaviour of the system. The safe operating range is acquired using the nyquist plot. The output power overshoots incurred due to dynamic load changed are alleviated due to the improvement in the transient response of the FLC. The comprehensive simulation study and experimental validation demonstrate the effectiveness of the proposed configuration and its competency to perform under different operating conditions. The hardware complexity and simulation compatibility can be enhanced using a software interactive dSPACE controller.

References

- [1] J. Acero, J. M. Burdio, L. A. Barragan, D. Navarro, R. Alonso, J. R. Garcia, *et al.*, "The domestic induction heating appliance: An overview of recent research," in *Proc. IEEE. Appl. Power Electron. Conf. Expo*, 2008, pp. 651-657. <https://doi.org/10.1109/APEC.2008.4522791>.
- [2] N. Ha Pham, H. Fujita, K. Ozaki, and N. Uchida, "Phase Angle Control of High-Frequency Resonant Currents in a Multiple Inverter System for Zone-Control Induction Heating," *IEEE Trans. Power Electron.*, vol. 26, pp. 3357-3366, 2011. <https://doi.org/10.1109/TPEL.2011.2146278>.
- [3] L. Grajales and F. C. Lee, "Control system design and small-signal analysis of a phase-shift-controlled series-resonant inverter for induction heating," in *Proc. IEEE Power Electron. Spec. Conf*, 1995, pp. 450-456 vol.1. <https://doi.org/10.1109/PESC.1995.474849>.
- [4] S. Chudjuarjeen, A. Sangswang, and C. Koompai, "An Improved LLC Resonant Inverter for Induction-Heating Applications with Asymmetrical Control," *IEEE Trans. Ind. Electron.*, vol. 58, pp. 2915- 2925, 2011. <https://doi.org/10.1109/TIE.2010.2070779>.
- [5] J. Tian, G. Berger, T. Reimann, M. Scherf, and S. J. Petzoldt, "Design and Implementation of a FPGA-Based Controller for Resonant Inverters," in *Proc. IEEE Power Electron. Spec. Conf.*, 2016, pp. 779- 784.
- [6] P. Nam-Ju, L. Dong-Yun, and H. Dong-Seok, "A Power-Control Scheme With Constant Switching Frequency in Class-D Inverter for Induction-Heating Jar Application," *IEEE Trans. Ind. Electron.*, vol. 54, pp. 1252-1260, 2007. <https://doi.org/10.1109/TIE.2007.892741>.
- [7] A. Dominguez, L. A. Barragan, J. I. Artigas, A. Otin, I. Urriza and D. Navarro, Reduced-Order Models of Series Resonant Inverters in Induction Heating Applications, *IEEE Trans. Power Electron.* Vol32 pp. 2300-2311, 2017. <https://doi.org/10.1109/TPEL.2016.2559160>.
- [8] C. Branas, F. J. Azcondo, and R. Zane, "Power-Mode Control of Multiphase Resonant Electronic Ballast," *IEEE Trans. Ind. Electron.*, vol. 59, pp. 1770-1778, 2014. <https://doi.org/10.1109/TIE.2011.2112322>.
- [9] P. Ha Ngoc, H. Fujita, K. Ozaki, and N. Uchida, "Dynamic Analysis and Control for Resonant Currents in a Zone-Control Induction Heating System," *IEEE Trans. Power Electron.*, vol. 28, pp. 1297-1307, 2015.
- [10] O. Lucia, J. M. Burdio, L. A. Barragan, C. Carretero, and J. Acero, "Series Resonant Multiinverter with Discontinuous-Mode Control for Improved Light-Load Operation," *IEEE Trans. Ind. Electron.*, vol. 58, pp. 5163-5171, 2011. <https://doi.org/10.1109/TIE.2011.2126541>.
- [11] R. Boukenoui H. Salhi, R. Bradai, A. Mellit, , "A new intelligent MPPT method for stand-alone photovoltaic systems operating under fast transient variations of shading patterns," *Solar Energy*, Volume 124, Pages 124-142, 2016. <https://doi.org/10.1016/j.solener.2015.11.023>.
- [12] Platon Baltas, Marina Tortoreli, Paul E. Russell " Evaluation of power output for fixed and step tracking photovoltaic arrays" *Solar Energy*, Volume 37, Issue 2, Pages 147-163, 1986.
- [13] M. A. G. de Brito, L. Galotto, L. P. Sampaio, G. de Azevedo e Melo, and C. A. Canesin, "Evaluation of the Main MPPT Techniques for Photovoltaic Applications," *IEEE Trans. Ind. Electron.*, vol. 60, pp. 1156-1167, 2013. <https://doi.org/10.1109/TIE.2012.2198036>.
- [14] S. M. R. Kazmi, H. Goto, G. Hai-Jiao, and O. Ichinokura, "A Novel Algorithm for Fast and Efficient Speed-Sensorless Maximum Power Point Tracking in Wind Energy Conversion Systems," *IEEE Trans. Ind. Electron.*, vol. 58, pp. 29-36, 2011. <https://doi.org/10.1109/TIE.2010.2044732>.
- [15] Y. Jiang, J. A. Abu Qahouq, and T. Haskew, "Adaptive-Step-Size with Adaptive-Perturbation-Frequency Digital MPPT Controller for a Single-Sensor Photovoltaic Solar System," *IEEE Trans. Power Electron.*, vol.28, no.7, pp.3195-3205, July 2013. <https://doi.org/10.1109/TPEL.2012.2220158>.
- [16] 21. A. Namadmalan, Universal Tuning System for Series-Resonant Induction Heating Applications, *IEEE Trans. Ind. Electron.* Vol. 64, pp. 2801-2808, 2017. <https://doi.org/10.1109/TIE.2016.2638399>.
- [17] T. Mishima, S. Sakamoto and C. Ide, ZVS Phase-Shift PWM-Controlled Single-Stage Boost Full-Bridge AC-AC Converter for High-Frequency Induction Heating Applications, *IEEE Trans. Ind. Electron.* Vol. 64 pp. 2054-2061, 2017. <https://doi.org/10.1109/TIE.2016.2620098>.
- [18] S. Skogestad and I. Postlethwaite, *Multivariable Feedback Control: Analysis and Design*: Wiley-Interscience, 2005.